# Evaluation and Design of Large-Scale Solar Adsorption Cooling Systems Based on Energetic, Economic and Environmental Performance

*energies*

MDPI

*Article*

# Evaluation and Design of Large-Scale Solar Adsorption Cooling Systems Based on Energetic, Economic and Environmental Performance

**Abdullah Ahmed Bawazir [1,2] and Daniel Friedrich [1,*]**

[1] School of Engineering, Institute for Energy System, The University of Edinburgh, Colin Maclaurin Road, Edinburgh EH9 3DW, UK; a.a.bawazir@ed.ac.uk

[2] Energy and Water Research Institute, King Abdulaziz City for Science and Technology, P.O. Box 6086, Riyadh 11442, Saudi Arabia

* Correspondence: d.friedrich@ed.ac.uk; Tel.: +44-(0)131-6505662

**Abstract:** In hot and dry regions such as the Gulf Cooperation Council (GCC) countries, the cooling demand is often responsible for more than 70% of electricity consumption, which places a massive strain on the electricity grid and leads to significant emissions. Solar thermal driven Silica-Gel/Water adsorption chillers, used for space cooling, could provide low carbon emission cooling and reduce the reliance on grid electricity. However, a meticulous design is required to make this both economically and environmentally beneficial. This paper aims to evaluate the solar thermal adsorption chiller performance based on large-scale cooling demand through a TRNSYS simulation for 1 year of operation. The proposed system consists of two main parts: first, the solar loop with evacuated tube solar collectors; and second, the adsorption cooling system with a silica-gel/water adsorption chiller. A neighbourhood of 80 typical 197 $m^2$ villas in Riyadh, the capital city of the Kingdom of Saudi Arabia (KSA), was taken as a case study. The solar adsorption cycle's performance has been compared to the conventional vapour compression cycle in terms of energy, economic and environmental performance. In addition, a parametric study has been performed for the main design parameters. Results reveal that the system can reach a solar fraction of 96% with solar collector area of 5500 $m^2$ and a storage tank volume between 350 and 400 $m^3$. Furthermore, the annual energy cost can be reduced by 74% for the solar adsorption system compared to the conventional vapour compression cycle. Meanwhile, the $CO_2$ saving percentage for the solar adsorption cycle was approximately 75% compared to the conventional vapour compression cycle. Carefully designed solar thermal cooling systems can reduce greenhouse gas emissions while covering a large scale of cooling demands. This can reduce the strain on the electricity grid as well as greenhouse gas emissions.

**Keywords:** solar adsorption cooling; TRNSYS; collector tilt angle; parametric study; 3E comparison



**Citation:** Bawazir, A.A.; Friedrich, D. Evaluation and Design of Large-Scale Solar Adsorption Cooling Systems Based on Energetic, Economic and Environmental Performance. *Energies* **2022**, *15*, 2149. https://doi.org/10.3390/en15062149

Academic Editor: Adalgisa Sinicropi

Received: 9 February 2022
Accepted: 7 March 2022
Published: 15 March 2022



## 1. Introduction

In hot climatic regions, particularly in the Middle East and North Africa (MENA), there is a growing demand for air conditioning. This is due to the warming climate, increased internal loads in structures, and increased demand for thermal comfort by users; as a result, it is becoming one of the most significant sources of energy consumption [1]. Refrigeration cycles and, in particular, air-conditioning systems are playing an important role in domestic, agricultural and industrial sectors. It has been indicated by the International Institute of Refrigeration (IIR), there are roughly 3 billion refrigeration, air-conditioning, and heat pump (HP) systems in use globally [2]. Furthermore, the refrigeration industry utilises around 17% of all power used globally. Residential consumption accounts for over 45% of total consumption, making it one of the most energy-intensive sectors in the world [2].

Such statistics provided by the IIR give a clear indication on the importance of the decarbonisation of refrigeration cycles. For air conditioning systems, they can be classified

as thermally or mechanically driven. An adsorption heat pump is an example of thermal driven heat, has workability that can employ thermal energy such as solar energy and the process/waste heat generated by industrial applications. Adsorption heat pumps have several advantages, including lower running costs, almost no vibration and noise, and are more ecologically friendly.[3].

On the other hand, the mechanically driven vapour compression cycle is powered by electricity, which strongly increases electricity consumption and emissions because most electricity is generated from fossil fuels in the Gulf Cooperation Council (GCC) region [4]. The high consumption of electricity is a significant problem for vapour compression refrigeration systems [5]: using fossil fuels for electricity production increases the release of greenhouse gas emissions into the environment, and the increasing electricity demand from the cooling side exacerbates power shortage problems. For that purpose, renewable energies such as wind and, especially, solar can play an important role, especially in the MENA and GCC regions. Countries in the MENA and GCC regions have some of the highest solar insolation in the world (approximately 6–8 kWh/m$^2$/day), with sunshine hours estimated to be 3600 h/year [6]. Thus, the integration of solar energy into power and refrigeration systems is considered advisable from both energy security and environmental viewpoints.

It has been shown by many studies that the combination of solar energy and adsorption cycles is a promising alternative for desalination, refrigeration, chilled water cooling, and air conditioning applications. Du et al. [7] optimised the solar collector area as heat source for adsorption desalination. The price is roughly CNY 0.03–0.04 per MJ, which is substantially cheaper than traditional energy sources and reduces the cost of the desalination. Reda et al. [8] presented a solar adsorption system on a residential scale for the location of Assiut, Egypt. The adsorption system uses a Silica-Gel/Water working pair and is driven by highly efficient evacuated tube solar collectors. In their work [8], the initial cost of the proposed systems ranged from EUR 2897/kWc to EUR 4808/kWc and the running costs over a year ranged from EUR 13.9/kWc to EUR 99.11/kWc. Palomba et al. [9] evaluated the performance of two 8.5 kW Silica-Gel/Water adsorption chillers working between 55 °C to 95 °C and driven by a 150 m$^2$ U-tube evacuated tube solar collector. Angrisani et al. [10] used TRNSYS to simulate an adsorption cooling system and compared flat plate and evacuated tube collectors based on the solar fraction. In addition, they compared the solar-driven system to a conventional system in terms of economic and environmental impact. The solar-driven system reduced primary energy consumption, was competitive for high energy prices and lowered comparable carbon dioxide emissions by more than 23%. In addition, they performed an economic analysis comparing the solar-driven system to a conventional system. Moreover, many other studies were presented [11–14] which investigated the performance of using different solar collectors on the adsorption cycles under various operating conditions.

In addition to the evaluation of different system configurations, it is essential to evaluate the system under different climatic and operating conditions. The performance of solar adsorption systems under different climates was evaluated by Alahmer et al. [15]. They achieved average system coefficient of performance (*COP*) of 0.491 and 0.467 for Perth and Amman weather conditions, respectively, and with compound parabolic collectors (*CPC*) with an area of 36 m$^2$. Mehmood et al. [16] developed a simulation model based on energy, economic, and environmental criteria. A simulation model of solar-driven vapour absorption chillers was built and compared to vapour compression chillers in Pakistan's main cities. They found that the solar driven *ACS* had lower operating costs and $CO_2$ emissions than the water-cooled *VCC* by 4.1 and 3.19 times, respectively.

Besides the optimisation of the system integration, a number of studies are working on increasing the performance of the adsorption chiller component. Liu et al. [17] experimentally studied the performance of a glass–metal vacuum tube as the adsorption bed with a parabolic trough collector for thermally driven adsorption cooling in summer, while in winter the thermal collector was used as a heat collector source of heating. They

reported a system level *COP* of 0.329 and investigated a number of methods to improve the system performance. Basdanis et al. [18] investigated different half-cycle durations of the adsorption chiller in two scenarios: first, a constant duration and, second, a duration that changes dynamically with solar radiation intensity. The dynamically optimised half-cycle duration can increase the daily and monthly cooling capacity by around 12%.

It is clear from the literature that solar thermal energy has significant potential to drive adsorption cycles. However, most of the literature is focused on small-scale or domestic use. On the other hand in Riyadh, a group of 80 villas investigated under the hot and dry climate of the capital city of Saudi Arabia was used as a case study. In conjunction with its high solar irradiation, Saudi Arabia's new strategy focuses on renewable solar technology to meet the significant growth of rising annual electricity demand. Furthermore, residential complexes account for 15% of total electricity use [19].

This study aims to model and simulate a large-scale adsorption chiller operating in the desert climate. In contrast to many studies which only evaluate the energetic performance, the large-scale system will be evaluated with respect to its energy, economic and environmental performance. The cooling system contains two main parts which are: (i) Solar evacuated tube collector (*ETC*) and (ii) Adsorption chiller cycle (*ADC*) using Silica-Gel/Water as the adsorbent/adsorbate pair. This study will present the following four contributions:

- The proposed system will be modelled and evaluated based on the operating conditions for Riyadh, KSA, where the load data will cover one year of operation for a neighbourhood of 80 villas. The villas will be modelled in SketchUp™ software [20] and TRNBuild [21]. The resulting cooling load of the neighbourhood is given as a time series with a maximum load of 2 MWth;
- A dynamic simulation model of the solar-driven adsorption chiller system and a conventional vapour compression cycle system will be implemented in TRNSYS 18 [21]. The model will be used to investigate and compare the systems in terms of their energetic, economic and environmental performance;
- A parametric study will evaluate the effects of solar radiation, storage volume, auxiliary heat set point, solar collector tilt angle and solar collector area on the system performance. The results will be used to identify the best configuration in terms of energy consumption and costs;
- The performance of a system with high solar fraction will be demonstrated based on the different temperatures and energy flows during the summer days with the highest cooling demand.

## 2. System Description

This section presents the working principles of the solar-assisted vapour adsorption cooling system and the conventional vapour compression cycle.

### *2.1. Conventional Vapour Compression Cycle (VCC)*

The vapour compression refrigeration cycle transfers heat from a cold reservoir at low temperature to a hot reservoir at high temperature. The evaporator, compressor, condenser, and expansion valve are the four components of the basic cycle of the vapour compression refrigeration system, as shown in Figure 1.

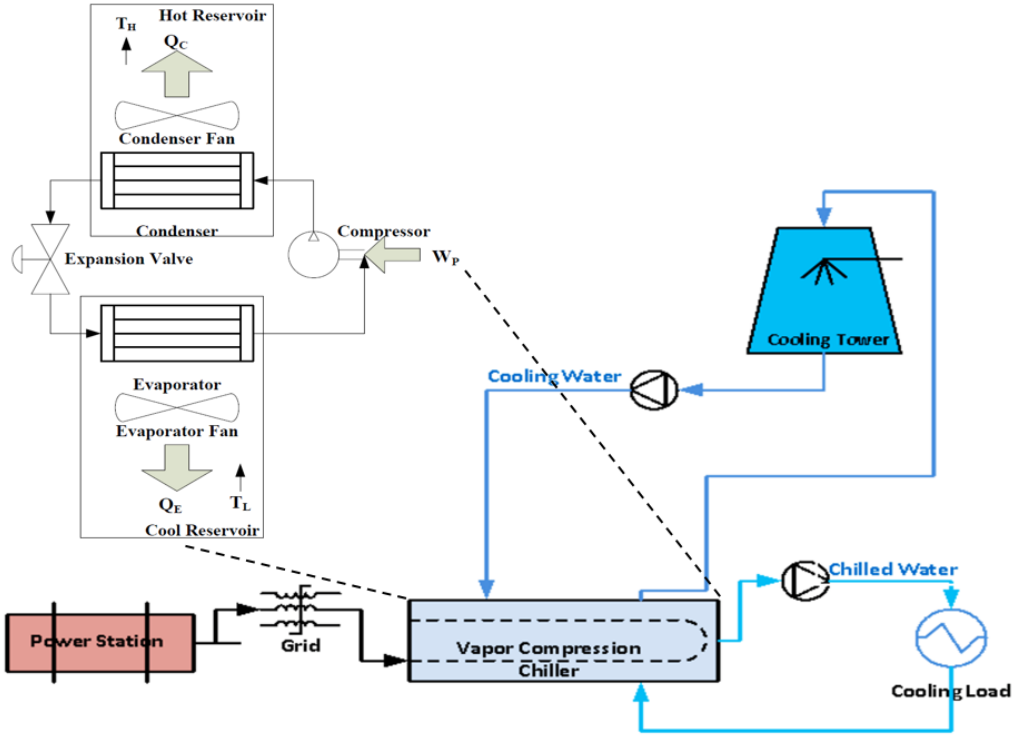


**Figure 1.** Schematic diagram of the basic cycle of a vapour compression refrigeration system.

The *VCC* components are linked in a closed loop so that the refrigerant can circulate continuously. The refrigerant enters the compressor via the intake and is compressed to a high pressure (condenser pressure). The refrigerant leaving the compressor is still in the gas phase, but it is at a high pressure and temperature. After the compressor, the superheated vapour reaches the condenser where it rejects heat to the secondary fluid that is coming from the cooling tower and has a lower temperature. A mechanical draft of a cooling tower will be used to cool down the condenser temperature. At the exit of the condenser the refrigerant temperature is below the condensation temperature so that it is a saturated liquid. The refrigerant in the liquid phase enters the expansion valve, where it is partly evaporated due to the rapid reduction in pressure. After the expansion valve the refrigerant is a two-phase fluid at a lower temperature and pressure. This fluid, which has a lower temperature than the cold reservoir, enters the evaporator where it completely evaporates at the evaporation temperature and by transferring heat energy from the cold reservoir to the refrigerant. After the evaporator, the refrigerant which is slightly above the evaporating temperature to ensure the safe operation of the compressor, enters the compressor and the cycle starts anew.

### *2.2. Solar Adsorption Cooling System (ADC)*

Figure 2 shows a schematic diagram of the solar adsorption cooling (*ADC*) system. A solar thermal driven adsorption bed substitutes the compressor in the solar *ADC* system, which is otherwise comparable to the *VCC* system. In contrast to the compressor in the *VCC* system, the adsorption bed operates in a cyclic manner with two main steps: first, during the adsorption step the adsorption bed, which is connected to the evaporator and kept at a low temperature, keeps the pressure low by adsorbing the evaporated refrigerant; second, during the desorption step the adsorption bed which is now connected to the condenser and kept at a high temperature, increases the pressure due to the desorption of the refrigerant. The minimum and maximum of the adsorbed refrigerant depends on the adsorption and desorption pressures and temperatures [22]. Moreover, the adsorbed content of refrigerants varies cyclically, depending on the adsorbent temperature and

system pressure, which varies between a maximum limit set by the condensation pressure and a minimum limit imposed by the evaporation pressure [22]. However in this work, the solar part is separated from the adsorption system.

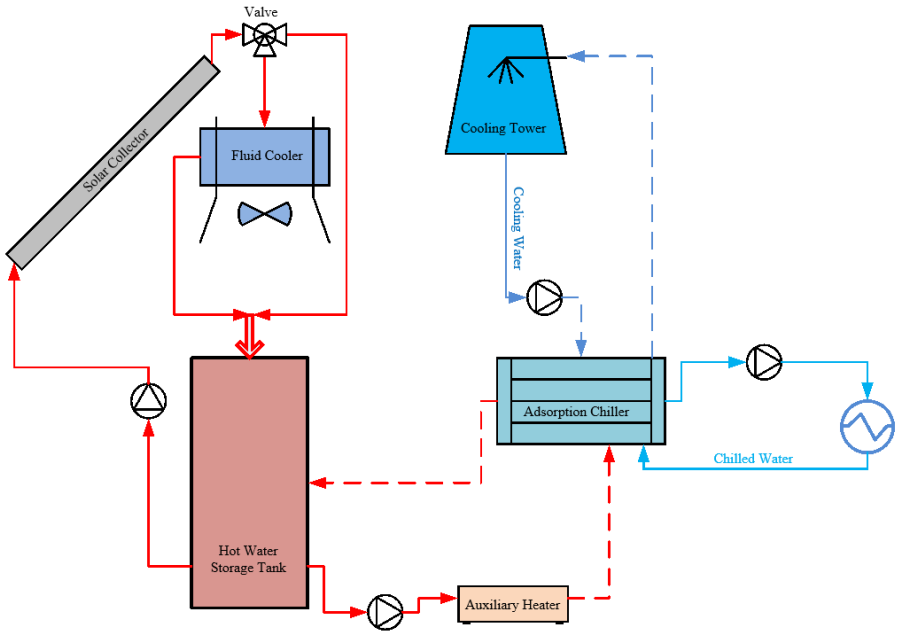


**Figure 2.** A schematic diagram of a solar adsorption cooling system.

Therefore, the system mainly consists of two major parts. The first is the solar loop, and the second part is the adsorption chiller, which is responsible for the chilled load application. The solar loop includes solar evacuated tube collectors for thermal energy collection, a fluid cooler to prevent any overheating, a storage tank to sustain thermal energy, and a circulation pump to overcome the pressure losses. The storage tank acts as a link between the solar loop and the adsorption cooling system. It receives the thermal energy from the solar loop and transfers the thermal energy towards the adsorption cooling system. Water is the primary working fluid in the solar loop. The adsorption chiller contains adsorber beds, which are filled with silica gel, a condenser unit for the condensation process, and the evaporative cooler for the chilled water process to the end-user. An auxiliary heater is included to provide the adsorbent bed with thermal energy if the solar loop cannot provide sufficient thermal energy. A mechanical draft cooling tower is used to cool down the condenser temperature and reject heat from the adsorption bed.

## 3. TRNSYS Model and Assumptions

This section describes the modelling environment, the developed system model as well as the performance metrics.

### *3.1. The Modelling Toolbox Environment*

The evaluation and performance analysis of the cooling system requires a software toolbox that can handle the complex interactions between the different units. In this work, the modelling and simulation tool TRNSYS 18 [21] has been used to simulate the performance of the proposed systems. The TRNSYS 18 toolbox is a very flexible software environment with a graphical user interface for the simulation of transient systems, in particular energy systems. It contains many thermal systems that can be easily combined in a graphical user interface. Meanwhile, the individual units were all validated and could, therefore, be implemented directly with confidence [21]. The system is designed to meet a cooling load in the range of 1300–2000 kW for Riyadh in Saudi Arabia. The flow chart in Figure 3 shows that the data from the building (cooling load), and the weather conditions are embedded in the TRNSYS code.

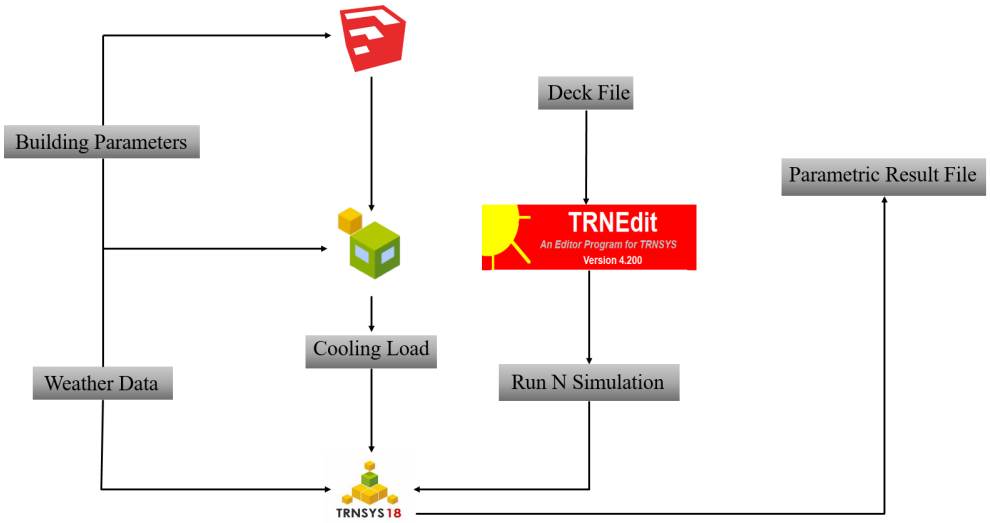


**Figure 3.** A schematic diagram of the flow chart for the modelling process via the TRNSYS toolbox.

### *3.2. System Description*

The TRNSYS schematic of the adsorption chiller driven by solar thermal energy and the four fluid loops is shown in Figure 4. The system consists of an adsorption cooling system, solar collector loop, hot water loop (*HW*), cooling water loop (*CW*), and chilled water loop (*CHW*).

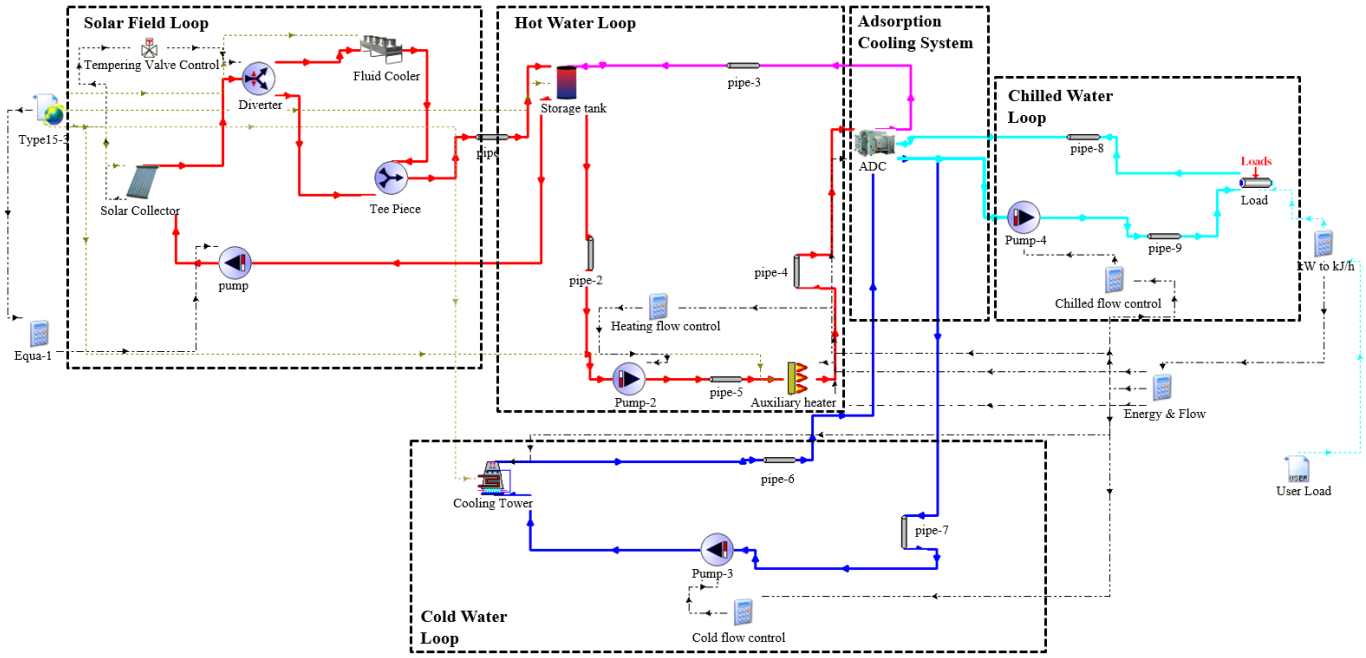


**Figure 4.** TRNSYS schematic of the proposed solar adsorption chiller system showing the different parts of the system.

The adsorption chiller (Type 909) receives hot fluid between 60 °C to 95 °C from the thermal storage tank to the silica-gel bed to desorp the refrigerant from the bed. The shared storage tank (Type 158) is a commonly adopted configuration between the absorption chiller loop and the solar collector [23]. The purpose of the evacuated tube collector (Type 71) is to provide thermal energy to the system. When the solar radiation is high, and the cooling demand is low, the evacuated tube collector is likely to overheat. However, when the fluid temperature in the solar system is above 120 °C, the tempering valve control (Type 953) with a fluid cooler (Type 511) can be applied to avoid overheating of the solar collectors.

The tempering valve control takes the tempered fluid set point temperature, 90 °C, and the fluid cooler models a dry fluid cooler which blows air across the coils containing the liquid.

If the hot water temperature at the storage tank exit remains below the specified value, the auxiliary heater (Type 659) will be switched on and will raise the fluid temperature to the required temperature. This hot fluid is used to desorb the refrigerant which regenerates the adsorption bed for the next cycle. The hot fluid returned from the adsorption chiller is pumped into the storage tank. A variable speed flow control is used to control the thermal energy delivered to the adsorption chiller from the storage tank. The fluid flow rate between the solar collector and the storage tank is controlled by an equation controller, which controls the variable speed pump (Type 110), but is only open when the solar irradiance exceeds a lower limit; this saves electrical consumption during times of low solar irradiance.

The chilled fluid is then passed through a load reader (Type 682), which imposes a user-specified load to fulfill the compound cooling profile of a small neighborhoods of 80 villas. A cooling tower is used to reject the heat of condensation and of the adsorption of the refrigerant in the silica-gel bed. The mathematical models implemented in TRNSYS which are based on thermodynamic equations, mass and energy balances can be found in the TRNSYS documentation.

Additionally, Figure 5 presents the TRNSYS model of the conventional, electricity driven *VCC* (Type 666). As described in Section 2.1, the conventional *VCC* generates chilled water, which is passed through a load reader (Type 682) to provide the cooling load of the buildings. The heat from the condenser is rejected through a cooling tower.

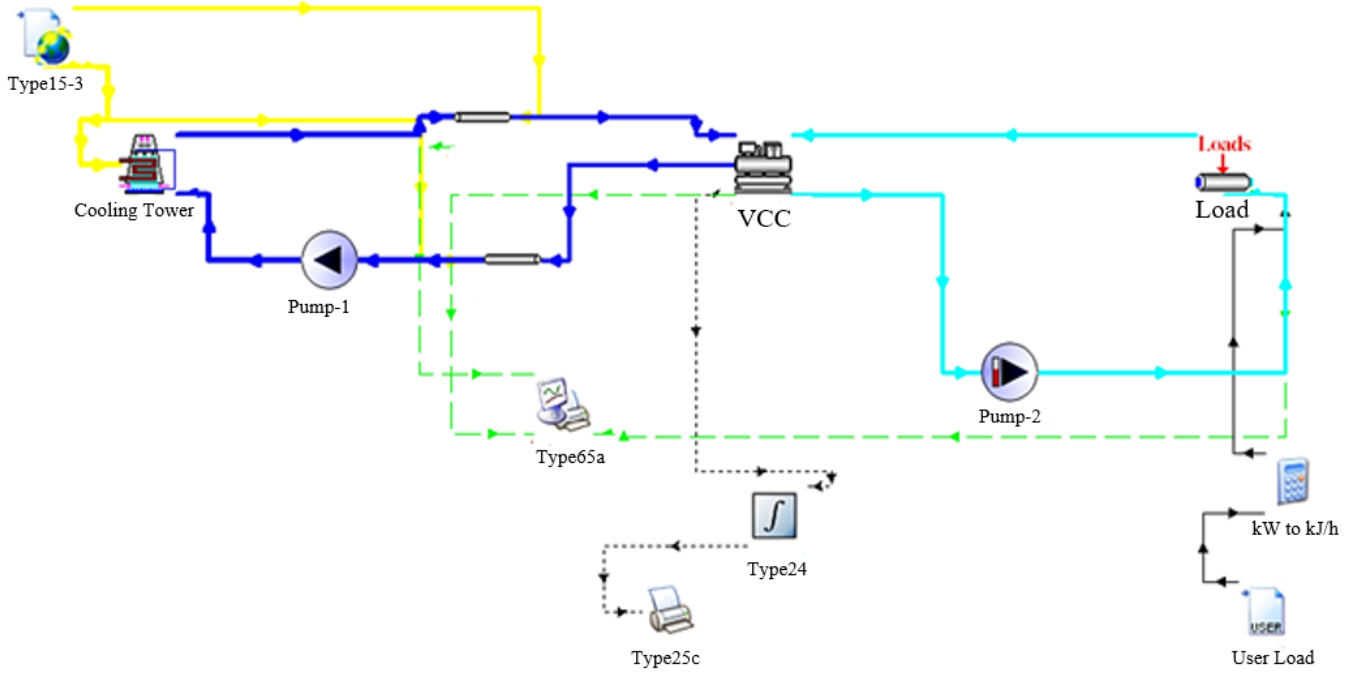


**Figure 5.** TRNSYS schematic of the proposed conventional vapour compression chiller for air conditioning showing the different parts of the system.

### *3.3. The Building Model and Weather Conditions*

The buildings considered in the present work are duplex family houses (villa) chosen from housing projects of the Saudi Ministry of Housing Department based on the "Saudi Arabia Standard Thermal Transmittance Values for Residential Buildings" [24]. The new requirements for the U-values for walls, roofs, and windows were adopted for the chosen villa as extracted from [24]. Following the Saudi Arabia Climate Zones classification, Riyadh is located in Zone 1 and, therefore, the following analysis uses the values for Zone 1 [24].

The building model was established based on an actual medium-sized building with two floors, as shown in Table 1. The first floor is 108 $m^2$, and the second floor is 89 $m^2$, while the building's total height is 6 m. A 3-dimensional design of the property was produced using the SketchUp™ software [20] to import the geometric information of the villa into the TRNBuild environment (see Figure 6). The duplex house (villa) construction specifications for the base-case energy model were set up in TRNSYS as Type 682.

**Table 1.** Duplex house (villa) construction specifications extracted from [24].

| Parameter | Description | Parameter | Description |
|---|---|---|---|
| First floor | 108 $m^2$ | Relative Humidity | 50% |
| Second floor bedrooms | 89 $m^2$ | U External walls | 0.34 $W/m^2$ K |
| Total height | 6 m | U Internal partition | 1.639 $W/m^2$ K |
| Gross floor area | 197 $m^2$ | U Intermediate floor | 2.923 $W/m^2$ K |
| Gross wall area | 241.65 $m^2$ | U Roof | 0.25 $W/m^2$ K |
| Window area | 21.7 $m^2$ | U glazing | 0.598 $W/m^2$ K |
| Number of occupants | 6–10 people | Lighting. | 5 $W/m^2$ |
| Temperature set point | 24 °C | Appliances | 3.8 $W/m^2$ |

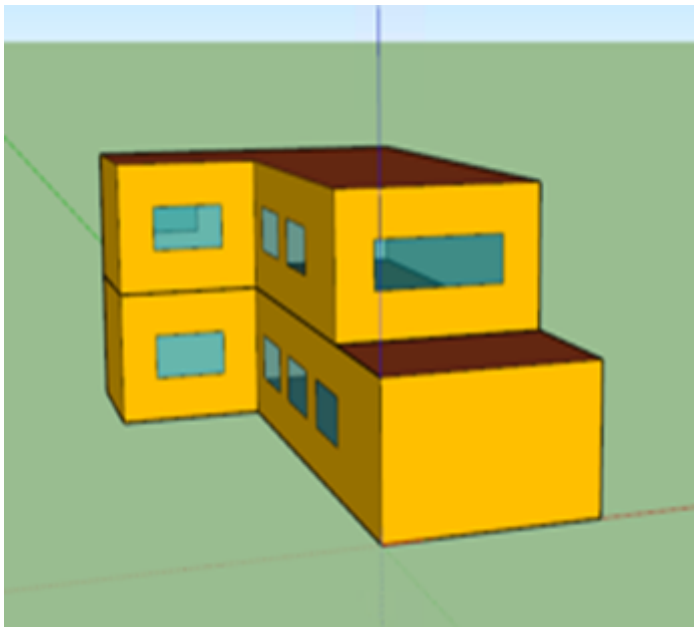

**Figure 6.** Building model (villa) made in SketchUp.

The cooling energy demand of the duplex family house (villa) was dynamically simulated in Riyadh, Saudi Arabia. The measured weather data consists of major meteorological parameters such as dry-bulb temperature and relative humidity. Ambient temperature data and global horizontal irradiance in hourly resolutions were taken from the TRNSYS data set. Table 2 summarises the annual mean temperature and global horizontal irradiance for the Riyadh location.

**Table 2.** Annual mean air temperature and global horizontal irradiance for Riyadh, Saudi Arabia.

| Location | Latitude–Longitude | Elevation | Global Horizontal Irradiance | Mean Ambient Temperature |
|---|---|---|---|---|
| Riyadh | N 24c 72′–E 46c 61′ | 688 m | 6.01 $kWh/m^2/day$ | 28.06 °C |

## 4. System Performance Indices

This section introduces the performance indices which will be used to evaluate the solar adsorption chiller system in comparison to the conventional vapour-compression chiller system. The parameter values for the performance indices are given in Table 3.

**Table 3.** Parameter values for the energy-related, economic and environmental (3E) analysis of the system. The values are extracted from the following references [13,16,25–29].

| Parameter | Unit | Value |
|---|---|---|
| Average business electricity price | USD/kWh | 0.08 |
| Average business natural gas price | USD/$m^3$/h | 0.013 |
| Interest discount rate (i) | % | 0.05 |
| Lifetime of the $ADC$ plant | year | 25 |
| Lifetime of the $VC$ system | year | 15 |
| Installation cost of $ADC$ | % of $CL_L$ | 150 |
| Installation cost of $VCC$ | % of $CL_L$ | 130 |
| Primary energy factor for electricity | $kWh_{PE}/kWh_E$ | 3.05 |
| Primary energy factor for natural gas | $kWh_{PE}/kWh_E$ | 1.22 |
| $CO_2$ emission factor for electricity grid | kg/MWh | 750 |
| $CO_2$ emission factor for natural gas | kg/MWh | 202 |

### *4.1. Energy Related Analysis*

The energy-related performance evaluation of $ADC$ systems often concentrates on the solar fraction ($SF$) which is the fraction of the total energy needed that can be provided from the solar source. In addition, this study also evaluates the nonrenewable primary energy required during the operation of the $ADC$ system. This enables us to calculate the primary energy savings ($PES$)compared to a conventional $VCC$ system for an identical cooling load. The reference system in this study is a conventional water-cooled mechanical chiller that produces chilled water during the cooling load required. The primary energy consumption ($PEC$) of the $ADC$ system and the reference $VCC$ system were computed to determine the $PES$. The main energy consumption of the solar-driven $ADC$ system ($PEC_{ADC}$)and the conventional $VCC$ system ($PEC_{VCC}$) can be expressed as:

$$PEC_{ADC} = (PEF_E \times E_E + PEF_{NG} \times E_{NG}) \quad (1)$$

$$PEC_{VCC} = (PEF_E \times E_E) \quad (2)$$

where $E_E$ and $E_{NG}$ are the annual demand of electricity and auxiliary heat from the natural gas boiler, and $PEF_E$ and $PEF_{NG}$ are the primary energy conversion factors for grid electricity and the auxiliary natural gas boiler, respectively. The primary energy savings $PES$ of the $ADC$ system are given by:

$$PES = (PEC_{VCC} - PEC_{ADC}) \quad (3)$$

### *4.2. Economic Analysis*

When compared to the traditional vapour compression cycle, solar-powered heating and cooling systems have a high initial investment and low operational expenses. The most major market hurdle for solar-powered cooling systems is the higher initial investment cost. The current study's economic analysis is based on levelised investment and operating costs. The capital costs of the cooling system can be split into equipment costs and installation costs. Therefore, the levelised capital cost ($CL_L$) can be computed by:

$$CL_L = (\sum Z_k + C_{INSTL}) \times CRF \quad (4)$$

where $(\sum Z_k)$ represents the sum of the capital cost of all components and denotes the installation cost. The capital recovery factor ($CRF$) must also be considered, which can be determined by:

$$CRF = \frac{i(1+i)^n}{(1+i)^n - 1} \tag{5}$$

where i is the average annual interest (discount) rate and n is the plant lifetime. The assumptions for the energy-related, economic and environmental (3E) analysis and the capital costs are given in Table 3.

### *4.3. The Fuel Running Cost*

The energy to drive the $ADC$ is provided by electricity, or a combination of electricity and natural gas, while the conventional $VVC$ is driven by electricity. The running costs are calculated based on the assumption that the $ADC$ uses electricity to drive pumps and fans, while natural gas is used to provide auxiliary energy to the hot water loop during the night-time and periods of insufficient solar irradiance. For the conventional $VVC$, however, electricity is used to run the compressor and the pumps. The annual cost of electricity and natural gas consumption can be calculated by:

$$FC_E = E_E \times c_E \tag{6}$$

$$FC_{NG} = E_{NG} \times c_{NG} \tag{7}$$

where $FC_E$ and $FC_{NG}$ represent the annual cost of electricity and natural gas consumption, while $E_E$, $E_{NG}$, $c_C$ and $c_{NG}$ represent the total electricity consumed, total natural gas consumed, the unit cost of electricity and unit cost of natural gas, respectively.

### *4.4. Environmental Analysis*

The energy to drive the $ADC$ is provided by electricity, or a combination of electricity and natural gas, while the conventional $VVC$ is driven by electricity. The annual $CO_2$ emissions can be calculated by:

$$CDE = CDE_E + CED_{NG} \tag{8}$$

where $CDE$ are the annual $CO_2$ emission based on the emissions from electricity and gas use calculated by:

$$CDE_E = E_E \times EF_{CO_2,E} \tag{9}$$

$$CDE_{NG} = E_{NG} \times EF_{CO_2,NG} \tag{10}$$

where $EF_{CO_2,E}$ and $EF_{CO_2,NG}$ are the $CO_2$ emission factors for grid and natural gas, which are listed in Table 3. These equations enable the calculation of the $CO_2$ emissions from both the adsorption chiller and vapour compression cycle systems.

### *4.5. System Assumptions*

The simulation of the complicated physical processes, e.g., adsorption chiller and solar collectors, and the streams in the different loops (see Figure 4) depends on a large number of assumptions which are listed in Table 4.

**Table 4.** Primary assumptions for the proposed solar adsorption cycle and vapour compression cycle systems. The values and parameters are extracted from the following references [23,30–35].

| Unit Process | Assigned Data |
| --- | --- |
| *ETC*/*ADC*:<br>- *ADS* working fluid is Silica-Gel–Water.<br>- Water is the main solar field working fluid. | Solar radiation, W/m$^2$ = varies throughout the year<br>Ambient temperature, 28 °C<br>*ETC* top temperature, 50–200 °C<br>*ETC* area, 4000–5500 m$^2$<br>*ETC* mass flow rate, 60–100 kg/s<br>*ETC* optical efficiency, 71%<br>Cooling load demand, 500–1400 kW<br>Load flow rate, 30–35 kg/s<br>User returned water temperature, 17–20 °C<br>Storage tank volume, 300–700 m$^3$<br>Cooling tower effectiveness, 60%<br>Pumping system efficiency, 75%<br>Plant lifetime, 20 years |
| - Vapour Compression Cycle (*VCC*): | Evaporator temperature, 5–10 °C<br>Condenser effectiveness, 80%<br>Cooling tower effectiveness, 60% |

In addition to these assumptions, the simulation depends on the sizes of the individual components and on the system boundaries such as inlet temperature, ambient temperature, and inlet cooling water temperature. These boundary values as well as the cooling load calculated for the villas defined in Table 1 are monitored and recorded during the model run. Based on these assumptions and boundary values, the system performance is simulated with an iterative algorithm that takes recycled and backward streams into account. The operational behaviour is used to calculate the energetic, economic and environmental performance of the systems. While this research focuses on the system operating expenses, we also compare the capital costs of the two cooling systems for the case study in Section 6.

## 5. Results and Discussion

This section presents an overview of the climatic conditions for Riyadh city in the Kingdom of Saudi Arabia, before evaluating a solar-driven adsorption chiller system with the aim to provide affordable and environmentally friendly cooling for a neighbourhood of 80 villas. The results show the optimal tilt angle for the solar collectors and perform a parametric study to find the best system configuration based on four performance metrics: solar fraction, primary energy saving, annual consumption cost, and savings of the $CO_2$ emissions. The parameters of the parametric study are given in Table 5.

**Table 5.** Parameters and ranges for the parametric study.

| | Unit | Minimum Value | Minimum Value |
| --- | --- | --- | --- |
| Evacuated Tube Solar Collectors | m$^2$ | 4000 | 5500 |
| Heat storage tank | m$^3$ | 100 | 700 |
| Auxiliary heat set point temperature | °C | 50 | 85 |
| Tilt angle Degree | $\beta$ | −90 | 90 |

### 5.1. Weather Conditions

Riyadh has a dry desert climate, with an average annual temperature of 28 °C and a relative humidity of 25%, according to the King Abdullah City for Atomic and Renewable Energy climate classification [33]. The hourly ambient dry bulb temperature and relative humidity are shown in Figure 7.

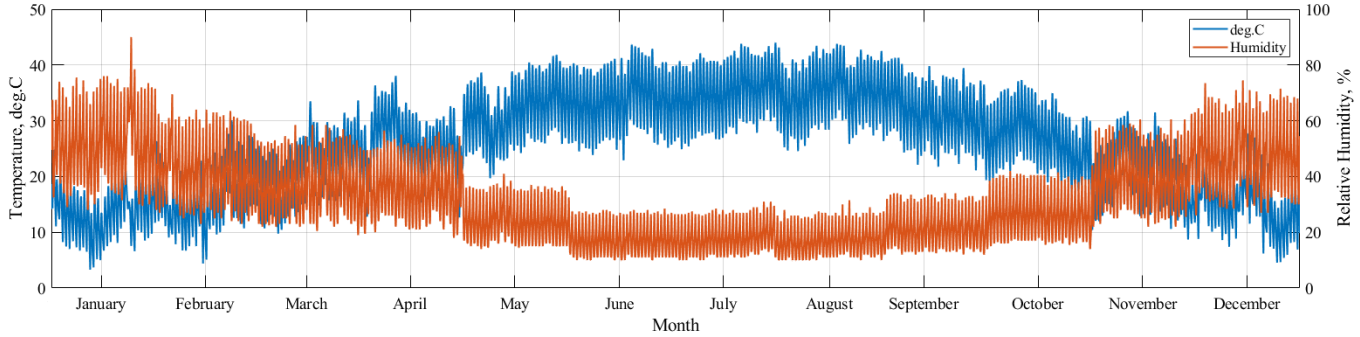


**Figure 7.** Ambient temperature and relative humidity for Riyadh, KSA generated with data from [33].

As anticipated, the dry bulb temperature increases during the summertime when it ranges between 30 °C to 42 °C. The lowest values for the dry bulb temperature were between 7 °C and 20 °C during winter. The relative humidity presents an inverse behaviour as shown in Figure 7 when compared to the dry-bulb temperature. During the winter season, the relative humidity ranges between 40 and 70%. However, dry conditions with relative humidity between 10 and 30% prevail during the summer season (April to October). Figure 7 shows that there is an urgent need for the cooling system to retain internal space in the comfort condition zone.

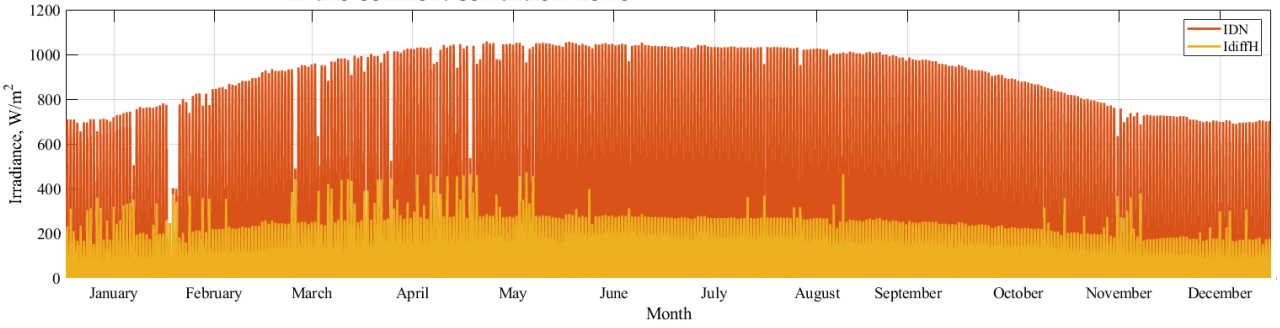


**Figure 8.** The hourly variation of solar radiation along the year for Riyadh, KSA generated with data from [33].

On the other hand, Riyadh has high solar radiation, as shown in Figure 8.The high solar radiation increases the reliability of solar driven systems. The maximum irradiance ($IDN$) exceeds 1100 W/m$^2$ while even the minimum average values are around 500 and 650 W/m$^2$ which is extremely viable for any solar thermal system. The diffuse solar radiation ($IdiffH$) displays a varying range between 100 and 250 W/m$^2$. As mentioned before, the proposed solar adsorption system will serve the building for the whole day (24 h) and throughout the year. However, during the winter season, the system is mostly switched off.

### *5.2. Tilt Angle Analysis*

The optimal solar collector tilt angle should be selected for the location of interest based on the solar radiation angle and the system performance. This is accomplished via a parametric study where the tilt angle is systematically changed while recording the available solar irradiation at the collector.

Figure 9 shows the monthly available solar energy for different tilt angles and for different months.

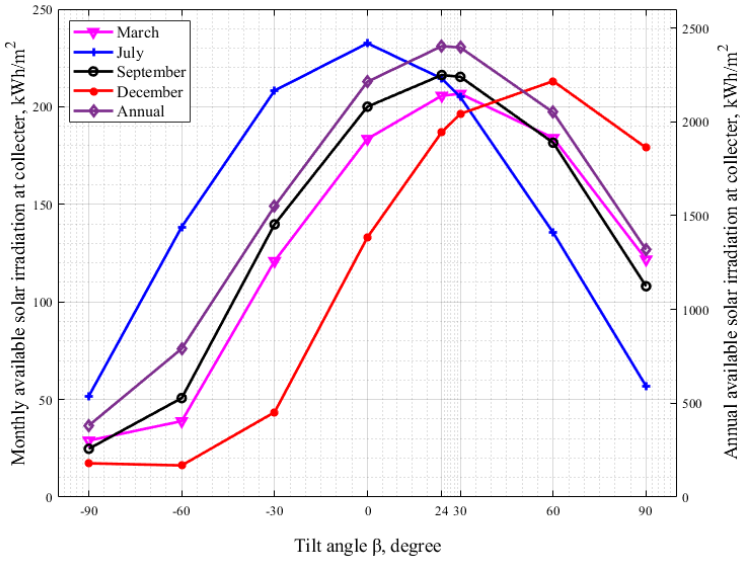


**Figure 9.** The effect of tilt of the solar irradiance as a function of collector tilt angle.

The right axis of Figure 9 shows the variation of annual solar irradiance available at the collector surface for different tilt angles. The maximal annual solar irradiance is available at the collector surface by setting the collector tilt angle to 24.7°. Setting the tilt angle at a higher or lower degree than this will reduce annual solar irradiance at the collector surface. The parametric study of monthly optimised tilt angle varies from 0° to 61° towards the south throughout the year. Figure 10 indicates that the maximum solar irradiance in the summer season is received at the collector by setting the collector at lower tilt angles and at higher tilt angles in the winter season.

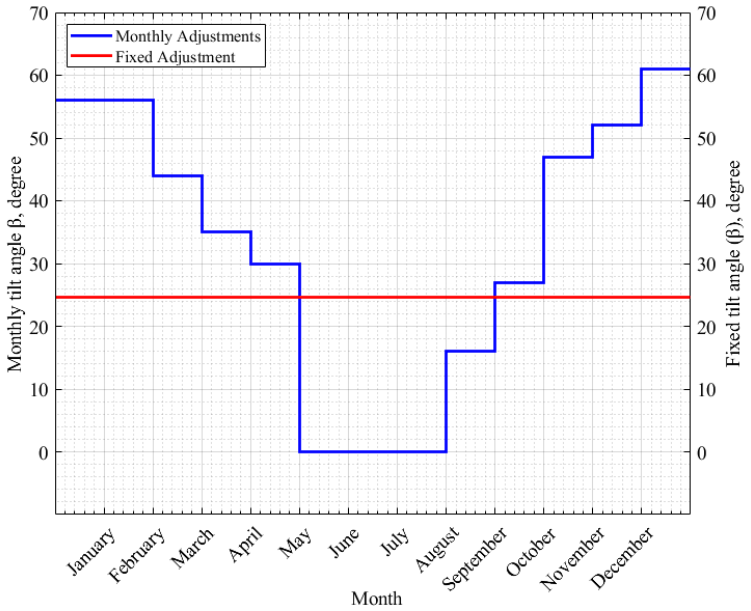


**Figure 10.** The variation of the optimal monthly tilt angle vs the optimal fixed tilt angle.

### *5.3. Building Energy Analysis*

A dynamic simulation of the building thermal behaviour was conducted on an hourly basis over a 1-year period with the model described in Section 3.3. Figure 11 shows both the monthly cooling requirement as well as the instantaneous cooling load.

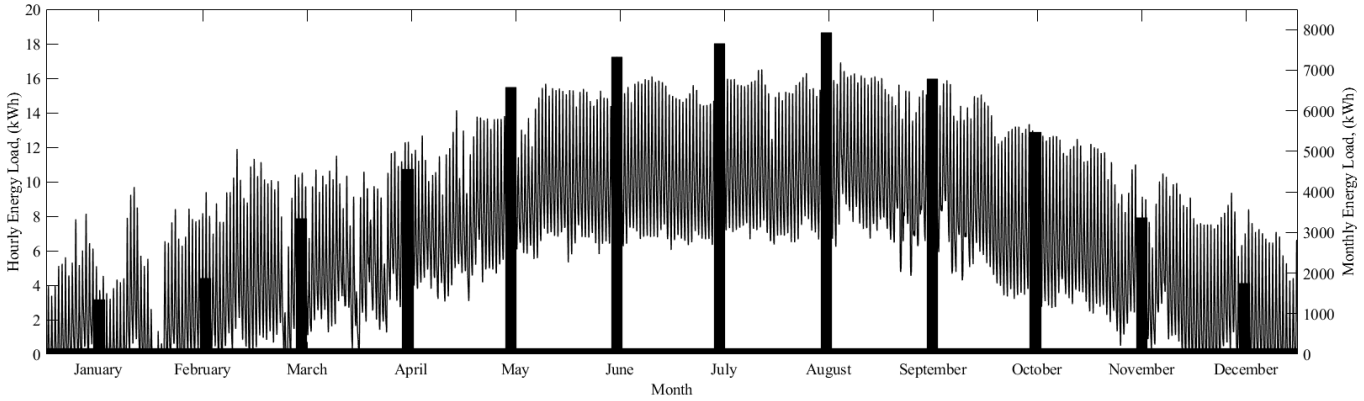


**Figure 11.** Hourly and monthly cooling load for a 197 $m^2$ villa in Riyadh, KSA.

The fluctuation depicts the hourly cooling demand, while the bars shows the seasonal change in cooling energy load. The hourly cooling load depicts not just seasonal fluctuations but also daily differences between day and night.

As for the validation of the simulation results [19], this was modelled on a villa in Riyadh following the same envelope characteristics as the Saudi Arabia thermal standard. The cooling load per unit area is 82.5 $W/m^2$, whereas it is 85 $W/m^2$ as per the present model. As is clear from Figure 11, the monthly demand is between 6000 kWh and 8000 kWh (30.4–40.4 $kWh/m^2$/month) during summertime. The minimum monthly demand loads were recorded during wintertime between 1500 kWh and 2000 kWh.

The main reason for this high cooling load is because a 24 h operation is in place compared to shorter operating times in the other works which follow the ASHRAE standards 90.2 [36] and 62.1 [37]. This shows that the required cooling power is in compliance with previously published studies while the cooling energy is higher due to the longer operational hours used in this study.

The high cooling demand in Saudi Arabia is due to several reasons: high dry bulb temperature and high solar radiation throughout the year. While Riyadh has reasonably low relative humidity, as seen in Figure 7, Saudi cities located closer to the sea have significantly higher relative humidity. This difference across the different regions of Saudi Arabia will be discussed in a future publication. The high cooling demand shows that Riyadh and the other cities in Saudi Arabia require efficient cooling systems. It is essential to evaluate the effect of different design aspects to achieve beneficial economic and environmental performance.

### *5.4. System Performance Analysis*

In this section, a parametric study on the system has been performed over the volume of the storage tank, the solar collector area, and the auxiliary heater set point.

Figure 12 shows the effect of the storage volume on the system solar fraction ($SF$) for various solar collector areas. Increasing the solar collector field area could increase the $SF$ up to 97% for an optimal storage volume of 300–400 $m^3$.

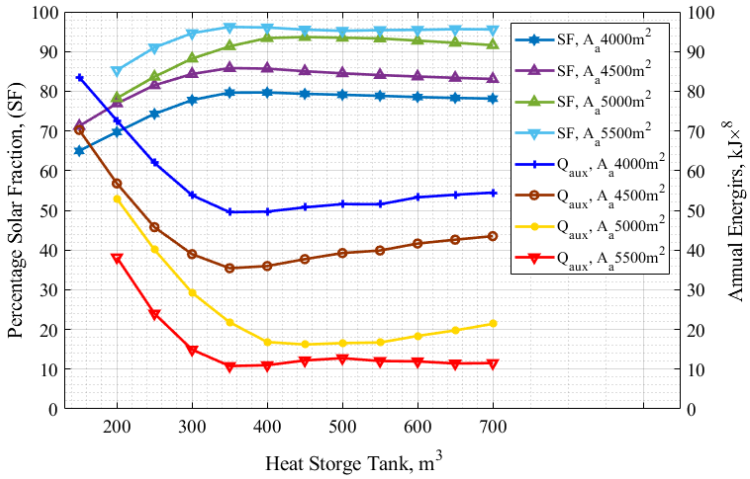


**Figure 12.** The solar fraction and annual auxiliary energy need vs the storage tank size for different solar field sizes.

As expected, the annual energy of the auxiliary heat was recorded at its lowest at a solar field size of 5500 $m^2$ and highest at a solar field size of 4000 $m^2$. It is interesting to note that for a fixed solar field size, the auxiliary energy demand increases for larger storage tank sizes. This is due to the increased thermal losses from the hot water storage tank as well as the nonoptimal temperature profile in the larger storage tanks. The annual auxiliary energy indicates that using a solar field of 4000 $m^2$ would need more thermal power to compensate the system demand, which would increase the cost and the $CO_2$ emissions. However, at 5500 $m^2$, the annual auxiliary energy would be supported by minimum power, as shown in Figure 12. As mentioned in this regard, the optimum storage volume should be kept between 350 and 500 $m^3$ for each case.

Figure 13 illustrates the variation of the SF against the auxiliary heater setpoint temperature.

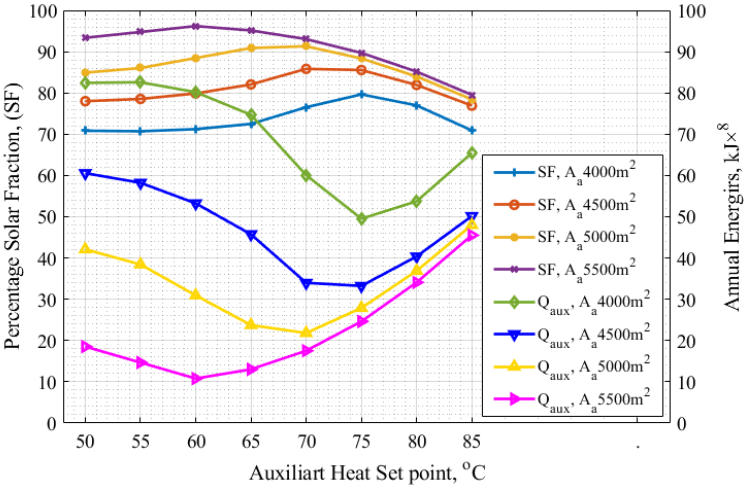


**Figure 13.** The solar fraction and annual auxiliary energy need vs. the auxiliary heat setpoint temperature for different solar field sizes and a storage volume of 350 $m^2$.

Initially, the solar fraction increased with the auxiliary setpoint temperature up to an optimum point and decreased with further increases of the setpoint temperature. The value of the optimum setpoint depends on the size of the solar field area and storage tank size, which here is fixed at 350 $m^2$, and should be in the range of 60–75 °C. Concurrently, the setpoint temperature of the auxiliary heater influences the energy provided by the auxiliary heater. This demonstrates the complex interaction between the supply and return

temperatures in the operation of solar-driven cooling systems. For example, if the setpoint temperature is too high, the hot water storage tank will be unable to absorb all the energy from the solar field, which will reduce the solar fraction. Figures 12 and 13 indicate the system viability throughout the year under different operating conditions.

Figure 14 represents contrasting monthly energy loads such as the cooling load, useful energy, and energy requirement for specific units such as adsorption chiller and cooling tower.

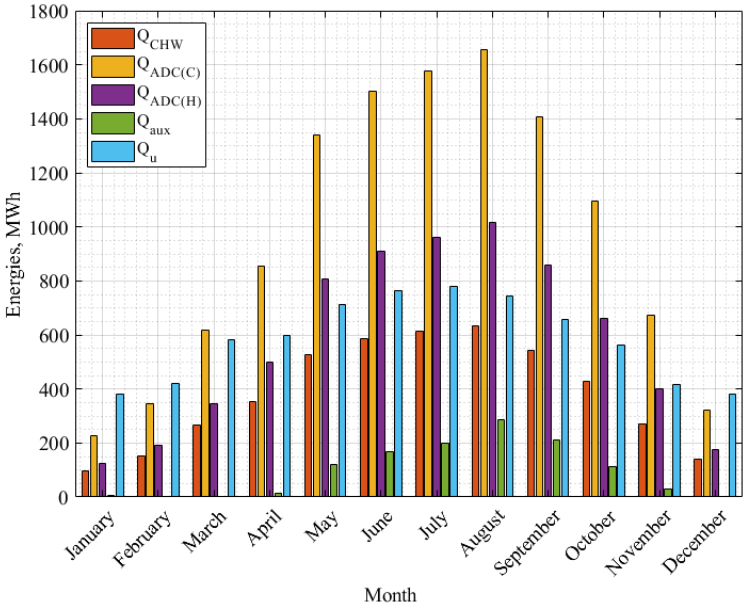


**Figure 14.** Monthly distribution of energies of the ADC system.

As shown in Figure 14, the energy load of the cooling tower is higher than the rest. The thermal power of the cooling tower is high because of the large amounts of heat that need to be rejected from the adsorption chiller. This would affect the system performance throughout the year besides the amount of $CO_2$ emission.

In the same regard, Figure 15 shows the monthly energy loads for the vapour compression cycle for 1 year.

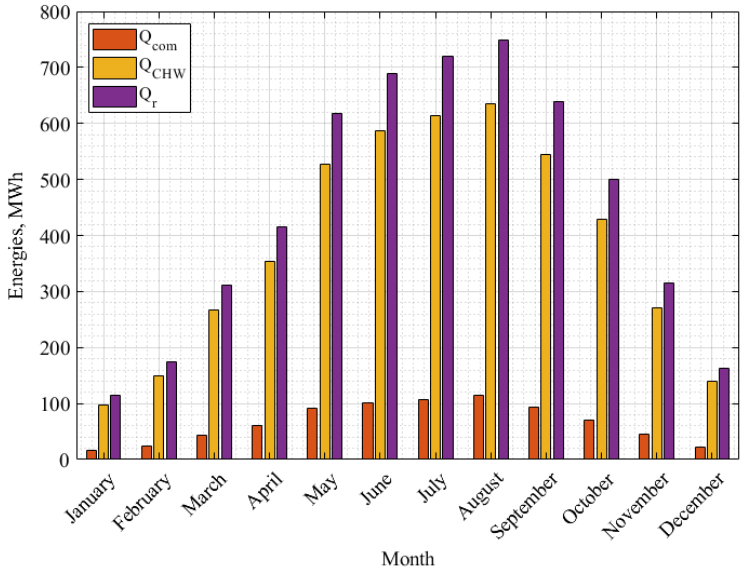


**Figure 15.** Monthly distribution of energies of the *VCC* system.

The figure shows the differences between load variations based on compressor power, chiller load, and heat rejection. It is demonstrated in Figure 15 that the chiller heat rejection is the highest load among the other units. Increasing the chiller load would be followed by an increase in the chiller heat rejection.

The monthly energy consumption of the pumps was calculated for the cases shown in Figures 14 and 15. The energy requirement for continuously operating pumps for the *ADC* system is around 20 MWh (depending on the exact pipe layout) and around half for the *VCC* system. The values for the *ADC* system are the worst case because the solar collector loop is not operating during the night time. While the *ADC* system has a higher pump energy requirement, these are significantly lower than the energy requirements to run the adsorption chiller or *VCC*.

Figure 16 shows the percentage of primary energy saving (*PES*) based on the solar collector area and the storage tank volume.

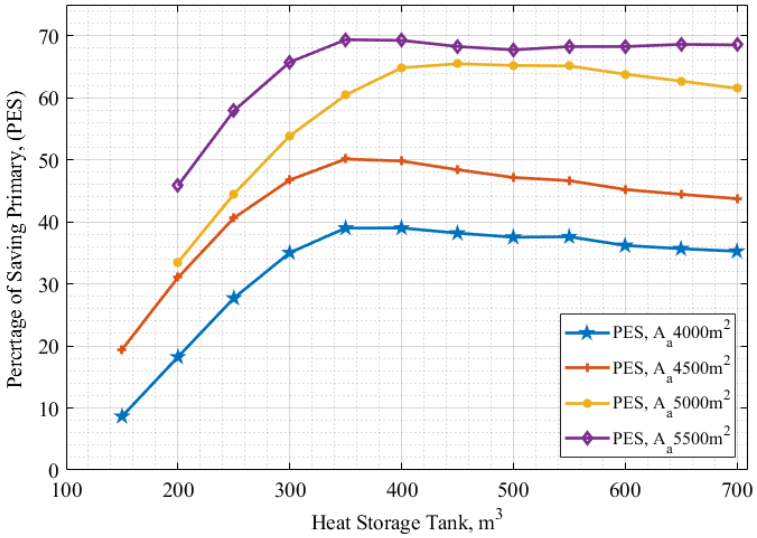


**Figure 16.** The primary energy saving of *ADC* unit vs *VCC* based on the storage tank volume and solar field area variations for an auxiliary set point temperature of 70 °C.

Increasing the storage tank volume would increase the *PES* up to 70% for 5500 $m^2$ of solar area. After this optimum point, *PES* does not increase further, and it is not beneficial to increase the storage tank volume further. For the test range of solar areas, a storage volume between 300–400 $m^3$ would be optimal. Figure 17 shows the percentage of savings in the annual operating costs of the *ADC* system compared to the *VCC* system for different solar fields and storage sizes.

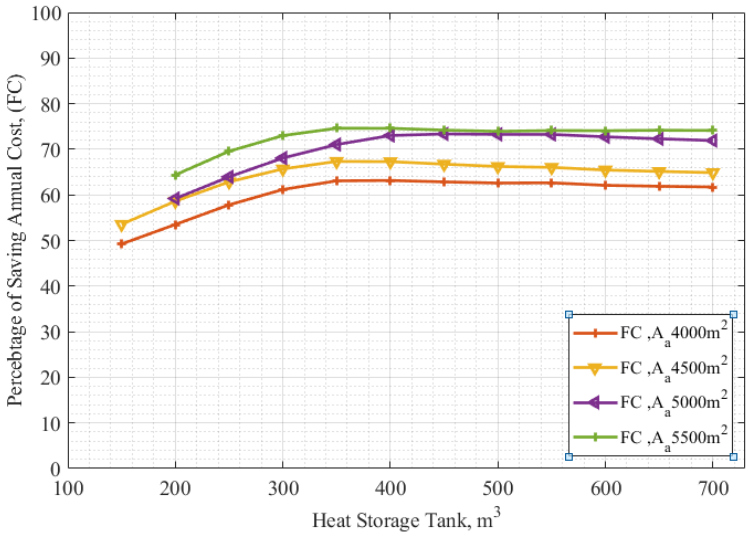


**Figure 17.** Savings of the annual operating cost of *ADC* unit vs *VCC* unit for the storage tank size and different solar field sizes for an auxiliary set point temperature of 70 °C.

By optimizing the storage tank size, the savings of the reported *ADC* would increase from 48% to 62% for a 4000 $m^2$ solar field size and from 64% to 75% for a 5500 $m^2$ solar field size. Increasing the storage volume will increase the percentage of saving to a certain limit. For the best evaluated case, the *ADC* system has a 69% lower primary energy consumption compared to the *VCC* system. The percentage of savings has been increased due to the indirect effect of the increased solar fraction. Although increasing the solar field area would increase the investment cost; a future study will optimise the levelised cost as well as the energy savings. For instance, the behaviour in Figure 17 shows an increasing trend from 150 $m^2$ up to 300 $m^2$. After that, the behaviour shows a nearly constant trend related to the volume increase. Accordingly, a value range of 300–400 $m^3$ should be adopted in this work.

As anticipated and based on the effect of the solar fraction coefficient, the percentage of saving at 5500 $m^2$ is the highest at 75%. On the other hand, at 4000 $m^2$ the percentage of saving is the lowest at about 45%. Figure 18 shows the effect of storage tank volume on the $CO_2$ saving percentage. These savings follow the same trends as the operational cost savings.

Figure 19 shows the percentage of energy provided by the solar field to achieve the required cooling energy. As mentioned earlier, a storage volume of 300–400 $m^3$ is optimal in that regard. For a solar field area of 5500 $m^2$, the percentage of energy from the solar field is about 85%. However, for a solar field area of 4000 $m^2$, the percentage of energy will drop to around 75%. Similarly, Figure 20 shows the percentage of energy provided by the solar field against the auxiliary setpoint temperature. As anticipated, increasing the auxiliary setpoint temperature from 50 °C to 85 °C will decrease the percentage of the energy provided by the solar field by around 15%.

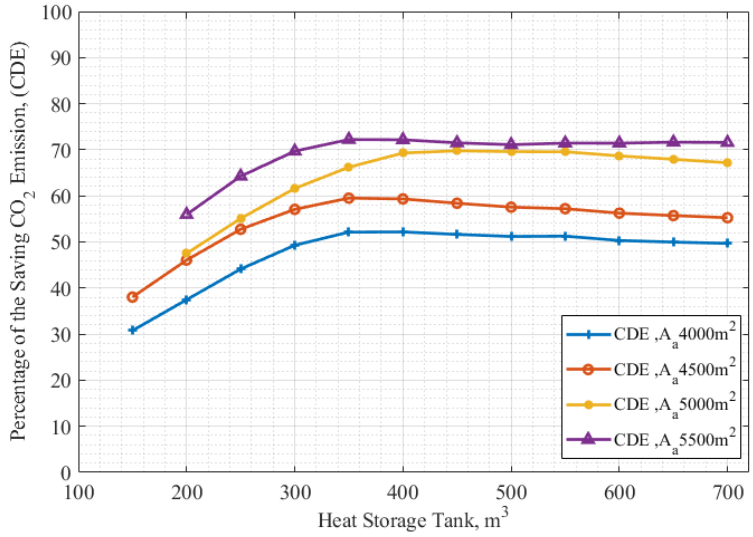


**Figure 18.** Savings of the $CO_2$ Emission of *ADC* unit vs. *VCC* unit for the storage tank size and different solar field sizes for an auxiliary setpoint temperature of 70 °C.

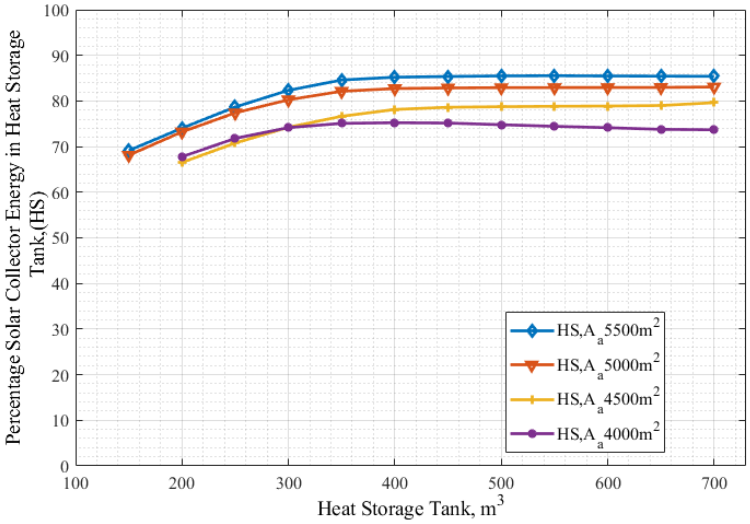


**Figure 19.** Percentage of energy from the solar field against the hot water storage volume for an auxiliary setpoint temperature of 70 °C.

Table 6 shows that both cooling systems share some mechanical components, such as a pump and a cooling tower. The *VCC* has approximately three times lower capital costs compared to *ADC* because the *ADC* system also needs a solar field, a evaporator, a condenser, and adsorbent beds, leading to its high capital cost, which consequently leads to a large increase on the investment cost. Because the larger investment cost is balanced by lower operational costs and environmental benefits, the profitability of solar *ADC* systems will depend, among other factors, on the cost of finance and carbon costs. This is beyond the scope of this study but will be handled in a future optimisation study.

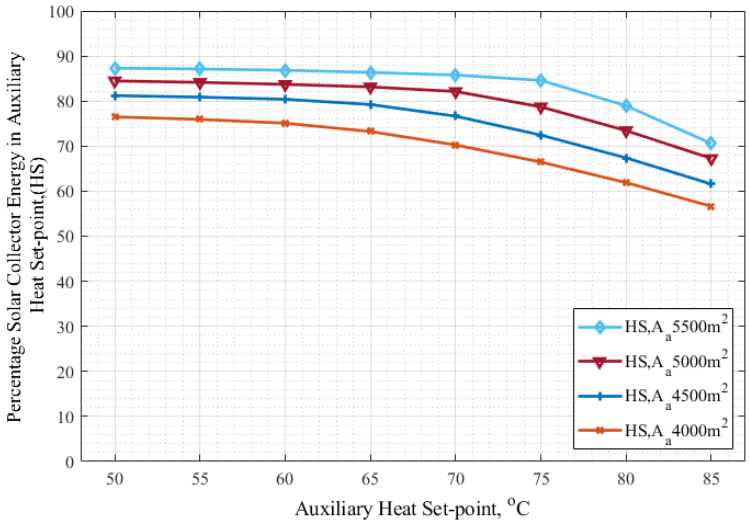


**Figure 20.** Percentage of energy from the solar field against the auxiliary set point for a heat storage tank of 350 $m^3$.

**Table 6.** The capital cost functions of the main components at a solar collector area of 5,000 $m^2$ and at a storage tank volume of 350 $m^3$ extracted from the following references volume [16,22,38–40].

| **Parameter**: | **Cost Function:** |
|---|---|
| *ADC*: | |
| *ETC* collector | 250 USD/$m^2$ |
| Hot water storage tank | 355 USD/$m^3$ |
| Auxiliary boiler | 700 USD/kW |
| Adsorption chiller | 475 USD/kW |
| Pump | 38 USD/kW |
| Cooling tower | 19 USD/kW |
| Fluid cooler | 19 USD/kW |
| *VCC*: | |
| Vapour compression chiller | 146 USD/kW |
| Cooling tower | 19 USD/kW |
| Pump | 38 USD/kW |

## 6. Case Study

As mentioned earlier, the solar field area and the storage tank affect the system's solar fraction, i.e., the levelised cost. For instance, a value of 5000 $m^2$ for the solar collection area and 350 $m^2$ of storage volume should be adopted in this case study. In this section, specific results were taken at the location of operation based on a typical day in summer to demonstrate the system case at specific points. The time of data extraction is in summer (27 July, 5 pm) and the peak dry bulb temperature is 45.9 °C. Table 7 shows the data results at the assigned day in the year.

It was discovered that 5 pm was the hour that maximum load demand occurred. The auxiliary heater setpoint was 70 °C and the flow rate through the solar field was approximately 70 kg/s, which is considered to be relatively high. The inlet and outlet solar field temperatures were 79.4 and 83.9 °C, respectively. The hot water flow rate through the hot water loop was approximately 43.5 kg/s, and the hot water temperature from the auxiliary heater towards the ADC was 84.6–85 °C. The returned outlet hot water temperature from the ADC was around 74.6 °C. For the cooling loop water cycle, the mass flow rate was approximately 77.5 kg/s, which reflects the massive heat rejection based on the significant amounts of load demand. The inlet cooling water temperature to the cooling tower was around 36 °C. As a general result, the chill energy needs were approximately 4569.49 MJ/h, the cooling needs were 11164.3 MJ/h and the hot energy needs were 6574.83 MJ/h. This is considered an important indication of the system's thermal power at this specific hour.

**Table 7.** The results of the *ADC*on a typical day/hour in summertime.

| Operating Conditions: |
| --- |
| 27 July, 5 pm<br>The peak dry bulb temperature, C 45.9 °C<br>The peak dry bulb temperature Time, h 4983 |
| Solar Field (*ETC*): |
| Solar collector area 5000 $m^2$<br>Tank volume 350 $m^2$<br>Auxiliary heater setpoint 70 °C<br>Flow rate in Solar field loop 70 kg/s<br>Temperature inlet to solar collector 79.4 °C<br>Temperature outlet from solar collector 83.9 °C<br>Temperature inlet to storage tank 83.9 °C |
| Cooling Water Loop: |
| Cooling water Flow rate 77.5 kg/s<br>Cooling water temperature inlet to cooling tower 36 °C<br>Cooling water temperature outlet to *ADC* 36.5 °C |
| Energy: |
| Chill energy needs 4569.4 MJ/h<br>Cooling energy needs 11164.3 MJ/h<br>Hot energy needs 6574.8 MJ/h<br>Energy from hot storage tank6471.1 MJ/h<br>Cooling tower Electricity consumption 35.9 MJ/h<br>*ADC* Electricity consumption 20.0 MJ/h |

Figure 21 shows a clear example over three consecutive days related to the temperature distribution and the energy flows through the system.

For instance, at sunrise, the temperature of the solar collector (in/out) displays sine curve behaviour as expected. During the night, the outlet stream from the solar collector declines gradually based on the effect of the storage tank leaving the auxiliary heat to take its place. The chilled water outlet from the *ADC* was observed to be almost constant based on the effect of the auxiliary heat throughout the day. The outlet hot water temperature from the *ADC* varied from 60 to 75 °C based on the effect of solar energy. Almost the same behaviour was noticed for the inlet solar field temperature. However, it remained constant during the night based on the effect of the auxiliary unit.

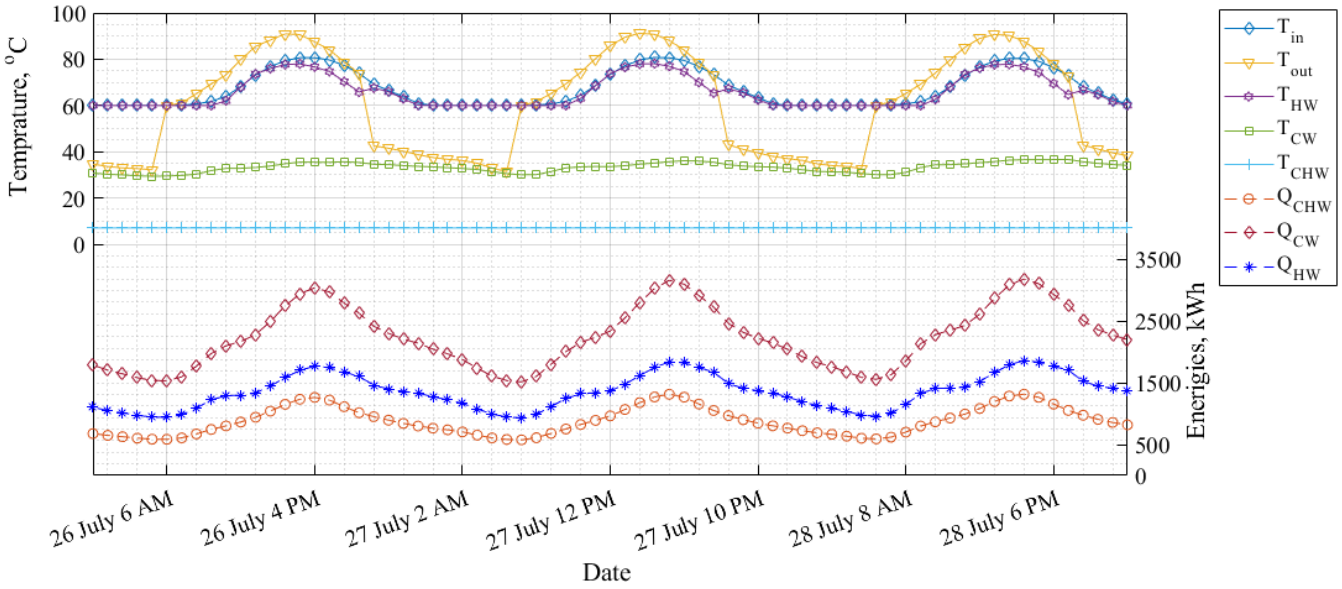


**Figure 21.** Temperature and energy distribution over three consecutive days during summertime *ADC*.

## 7. Conclusions

This work presents a design guideline for a 96% solar fraction adsorption cooling system in the desert climate of Riyadh, the capital of Saudi Arabia. Firstly, two models for the thermal-driven-based (solar-driven vapour adsorption chiller) and the vapour compression-cycle-based (water-cooled chiller) were modelled and simulated via the TRNSYS software toolbox for a range of system configurations including solar field, cooling plant, hot storage tank size and building cooling load. The hourly cooling water for 80 single-family villas in a residential compound in Riyadh was evaluated as a case study. Based on peak and hourly cooling load simulation, both systems have been compared for energy-related, economic, and environmental aspects for operating conditions of the desert climate. The coincidence of solar irradiance and extreme temperatures with the associated cooling demand makes solar thermal-driven cooling systems and, in particular, solar thermal-driven adsorption cooling systems especially suitable for locations in the MENA region.

The variable energy balance for both cooling systems were used to analyse and compare them. The results were compared to a conventional vapour compression cycle based on hourly load variations throughout the year. The results showed that the monthly demand values were in the range of 6000 to 8000 kWh during summertime for a 197 $m^2$ (case-study villa area) and the cooling load calculations per unit area were 85 $W/m^2$ as per the present model.

In addition, a parametric study was performed on the TRNSYS simulation model with the aim of developing design guidelines for a low-carbon cooling system. The main parameters affecting the performance of the adsorption cooling system such as collector area, storage tank volume, auxiliary heat setpoint, and solar collector tilt angles were investigated.

The parametric study showed that the optimum solar fraction can be achieved at 5500 $m^2$ of the solar collection area with a hot water storage tank of 300–400 $m^3$ and an auxiliary setpoint temperature between 65–70 °C. The cooling tower energy requirement is recorded as the highest among the solar adsorption chiller due to the high requirements for heat rejection of the adsorption system. The results demonstrate that the solar driven adsorption chiller can reduce the annual operating costs by up to 75% compared to a conventional vapour compression chiller system. The reduced operating costs and electricity demand compared to *VCC* systems makes *ADC* systems an interesting option in attempting to reduce cooling costs and emissions by up to 75%.

The study shows that solar driven adsorption cooling systems can significantly reduce the operational costs and $CO_2$ emissions of cooling system in the desert climate of Saudi Arabia. The widespread deployment of these systems can alleviate the strain on the electricity grid associated with an increasing cooling demand.

**Author Contributions:** Conceptualization, D.F.; Formal analysis, A.A.B. and D.F.; Investigation, A.A.B.; Methodology, A.A.B. and D.F.; Project administration, D.F.; Software, A.A.B.; Supervision, D.F.; Validation, A.A.B.; Visualization, A.A.B.; Writing – original draft, A.A.B.; Writing – review editing, D.F.

**Funding:** This research received no external funding.

**Acknowledgments:** Abdullah Ahmed Bawazir acknowledge Saudi Arabia Ministry of Higher Education in the form of PhD scholarship and King Abdulaziz City for Science and Technology (KACST).

**Conflicts of Interest:** The authors declare no conflict of interest.

## Nomenclature

| | |
|---|---|
| $PEC_{VCC}$ | The primary energy saving of Conventional vapour compression cycle |
| $PEC_{ADC}$ | The primary energy saving Solar adsorption cooling system |
| $PES$ | The primary energy saving($PEC_{VCC}$–$PEC_{ADC}$r) |
| $CDE_{NG}$ | annual $CO_2$ Emissions from natural gas (kg) |
| $CDE_E$ | annual $CO_2$ Emissions from electricity (kg) |
| $EF_{CO2,E}$ | Emission factors for grid |
| $EF_{CO2,NG}$ | Emission factors for natural gas |
| $E_E$ | Total the annual energy consumption of the electrical (kWh) |
| $E_{NG}$ | Total annual consumption of natural gas (kWh) |
| $FC_E$ | Annual cost of electricity (USD) |
| $FC_{NG}$ | Annual cost of natural gas (USD) |
| $CL_L$ | Levelised capital investment (USD) |
| $SF$ | Solar fraction |
| $CW$ | Cooled water |
| $CHW$ | Chilled water |
| $HW$ | Hot water |
| $ADC$ | Solar adsorption cooling system |
| $VCC$ | Conventional vapour compression cycle |
| $A_A$ | Collectors' absorber area($m^2$) |
| $T_H$ | High temperature region condenser (°C) |
| $T_L$ | Low temperature region evaporator (°C) |
| $W_p$ | Power in kW |
| $U$ | Overall heat transfer coefficient |
| $ETC$ | Evacuated tube collector |
| $c_E$ | Cost of electricity(USD) |
| $c_{NG}$ | Cost of natural gas (USD) |
| $\beta$ | Tilt angle of the panels (rad) |
| $Q_u$ | Useful energy gain from collector (kWh) |
| $Q_{aux}$ | Rate of energy delivered by auxiliary source (kWh) |
| $Q_{ADC(H)}$ | Rate of heat energy require ADC (kWh) |
| $Q_{ADC(C)}$ | Rate of cooling energy require ADC |
| $Q_{CHW}$ | Chilled water energy stream (kWh) |
| $Q_{HW}$ | Hourly thermal energy rate of hot water flow (kWh) |
| $Q_{CW}$ | Hourly thermal energy rate of Cooled water flow (kWh) |
| $Q_{Com}$ | Rate of energy compressor (kWh) |
| $Q_r$ | Rate of energy heat reject (kWh) |
| $Q_E$ | Heat removed from a low temperature region |
| $Q_C$ | Heat added to a high temperature region |
| $T_{in}$ | Hot water temperature inlet solar collector (°C) |
| $T_{out}$ | Hot water temperature out solar collector (°C) |
| $T_{CHW}$ | Chilled water temperature return (°C) |
| $T_{HW}$ | Hot water temperature return (°C) |
| $T_{CW}$ | Cold water temperature return (°C) |
| $COP$ | Coefficient of performance |
| $IDN$ | Hourly direct normal solar irradiance ($W/m^2$) |
| $IdiffH$ | Hourly diffuse horizontal solar irradiance ($W/m^2$) |
| $i$ | Interest discount rate |
| $n$ | Project lifetime (years) |

## References

1. Al-Falahi, A.; Alobaid, F.; Epple, B. A new design of an integrated solar absorption cooling system driven by an evacuated tube collector: A case study for Baghdad, Iraq. *Appl. Sci.* **2020**, *10*, 3622. https://doi.org/10.3390/app10103622.
2. Arteconi, A.; Polonra, F. Demand side management in refrigeration applications. *Int. J. Heat Technol.* **2017**, *35*, S58–S63. https://doi.org/10.18280/ijht.35Sp0108.
3. Gediz Ilis, G.; Demir, H.; Mobedi, M.; Baran Saha, B. A new adsorbent bed design: Optimization of geometric parameters and metal additive for the performance improvement. *Appl. Therm. Eng.* **2019**, *162*, 114270.

4. Osman, M.; Gachino, G.; Hoque, A. Electricity consumption and economic growth in the GCC countries: Panel data analysis. *Energy Policy* **2016**, *98*, 318–327. https://doi.org/10.1016/j.enpol.2016.07.050.
5. Goyal, P.; Baredar, P.; Mittal, A.; Siddiqui, A.R. Adsorption refrigeration technology - An overview of theory and its solar energy applications. *Renew. Sustain. Energy Rev.* **2016**, *53*, 1389–1410. https://doi.org/10.1016/j.rser.2015.09.027.
6. Nafey, A.S.; Sharaf, M.A. Combined solar organic Rankine cycle with reverse osmosis desalination process: Energy, exergy, and cost evaluations. *Renew. Energy* **2010**, *35*, 2571–2580. https://doi.org/10.1016/j.renene.2010.03.034.
7. Du, B.; Gao, J.; Zeng, L.; Su, X.; Zhang, X.; Yu, S.; Ma, H. Area optimization of solar collectors for adsorption desalination. *Sol. Energy* **2017**, *157*, 298–308. https://doi.org/10.1016/j.solener.2017.08.032.
8. Reda, A.M.; Ali, A.H.H.; Morsy, M.G.; Taha, I.S. Design optimization of a residential scale solar driven adsorption cooling system in upper Egypt based. *Energy Build.* **2016**, *130*, 843–856. https://doi.org/10.1016/j.enbuild.2016.09.011.
9. Palomba, V.; Vasta, S.; Freni, A.; Pan, Q.; Wang, R.; Zhai, X. Increasing the share of renewables through adsorption solar cooling: A validated case study. *Renew. Energy* **2017**, *110*, 126–140. https://doi.org/10.1016/j.renene.2016.12.016.
10. Angrisani, G.; Entchev, E.; Roselli, C.; Sasso, M.; Tariello, F.; Yaïci, W. Dynamic simulation of a solar heating and cooling system for an office building located in Southern Italy. *Appl. Therm. Eng.* **2016**, *103*, 377–390.
11. Yaïci, W.; Entchev, E. Coupled unsteady computational fluid dynamics with heat and mass transfer analysis of a solar/heat-powered adsorption cooling system for use in buildings. *Int. J. Heat Mass Transf.* **2019**, *144*, 1–17.
12. Fong, K.F.; Lee, C.K.; Chow, T.T.; Lin, Z.; Chan, L.S. Solar hybrid air-conditioning system for high temperature cooling in subtropical city. *Renew. Energy* **2010**, *35*, 2439–2451. https://doi.org/10.1016/j.renene.2010.02.024.
13. Shirazi, A.; Taylor, R.A.; White, S.D.; Morrison, G.L. Transient simulation and parametric study of solar-assisted heating and cooling absorption systems: An energetic, economic and environmental (3E) assessment. *Renew. Energy* **2016**, *86*, 955–971. https://doi.org/10.1016/j.renene.2015.09.014.
14. Islam, M.P.; Morimoto, T. Thermodynamic performances of a solar driven adsorption system. *Sol. Energy* **2016**, *139*, 266–277. https://doi.org/10.1016/j.solener.2016.09.003.
15. Alahmer, A.; Wang, X.; Al-Rbaihat, R.; Amanul Alam, K.C.; Saha, B.B. Performance evaluation of a solar adsorption chiller under different climatic conditions. *Appl. Energy* **2016**, *175*, 293–304. https://doi.org/10.1016/j.apenergy.2016.05.041.
16. Mehmood, S.; Maximov, S.A.; Chalmers, H.; Friedrich, D. Energetic, Economic and Environmental (3E) Assessment and Design of Solar-Powered HVAC Systems in Pakistan. *Energies* **2020**, *13*, 1–25. doi:10.3390/en13174333.
17. Liu, Y.; Yuan, Z.; Liu, Z. Experimental performance of a small solar system for adsorption cooling in summer and heating in winter. *J. Renew. Sustain. Energy* **2022**, *14*, 013702. https://doi.org/10.1063/5.0078181.
18. Basdanis, T.; Tsimpoukis, A.; Valougeorgis, D. Performance optimization of a solar adsorption chiller by dynamically adjusting the half-cycle time. *Renew. Energy* **2021**, *164*, 362–374. https://doi.org/10.1016/j.renene.2020.09.072.
19. Hmadi, M.; Mourtada, A.; Daou, R. Forecasting the performance of a district solar thermal smart network in desert climate—A case study. *Energy Convers. Manag.* **2020**, *207*, 112521. https://doi.org/10.1016/j.enconman.2020.112521.
20. SketchUp software, Trimble, Sunnyvale, California, USA, Available online: https://www.sketchup.com/industries/architecture (accessed on 23 April 2021).
21. TRNSYS (TRaNsient SYstem Simulation) software, University of Wisconsin-Madison and Thermal Energy System Specialists, Madison, WI, USA, 2017. Available online: http://www.trnsys.com (accessed on 15 November 2021).
22. Fernandes, M.S.; Brites, G.J.; Costa, J.J.; Gaspar, A.R.; Costa, V.A. Review and future trends of solar adsorption refrigeration systems. *Renew. Sustain. Energy Rev.* **2014**, *39*, 102–123. https://doi.org/10.1016/j.rser.2014.07.081.
23. Franchini, G.; Brumana, G.; Perdichizzi, A. Performance prediction of a solar district cooling system in Riyadh, Saudi Arabia—A case study. *Energy Convers. Manag.* **2018**, *166*, 372–384. https://doi.org/10.1016/j.enconman.2018.04.048.
24. Saudi Standards, Metrology and Quality Organization (SASO) Thermal Transmittance Values for Residential Buildings, SAUDI STANDARD DRAFT No. 28793/2014. Riyadh. https://saso.gov.sa/.
25. Saudi Electric Company. Available online: https://www.se.com.sa/en-us/Customers/Pages/TariffRates.aspx (accessed on 15 May 2021).
26. Global Petrol Prices. Available online: https://www.globalpetrolprices.com/Bahrain/natural_gas_prices/ (accessed on 18 May 2021).
27. CEIC. Available online: https://www.ceicdata.com/en/indicator/saudi-arabia/short-term-interest-rate (accessed on 10 May 2021).
28. Basrawi, F.; Ibrahim, T.K.; Lee, G.C.; Habib, K.; Ibrahim, H. Effect of Solar Fraction on the Economic and Environmental Performance of Solar Air-Conditioning by Adsorption Chiller in a Tropical Region. *J. Sol. Energy Eng. Trans. ASME* **2015**, *137*, 1–9. https://doi.org/10.1115/1.4031707.
29. Carbon Footprint. Country Specific Electricity Grid Greenhouse Gas Emissions. Available online: www.carbonfootprint.com (access on 15 November 2021).
30. Sharaf, M.A. Thermo-economic comparisons of different types of solar desalination processes. *J. Sol. Energy Eng. Trans. ASME* **2012**, *134*, 031001. https://doi.org/10.1115/1.4005752.
31. Castro, M.M.; Song, T.W.; Pinto, J.M. Minimization of operational costs in cooling water systems. *Chem. Eng. Res. Des.* **2000**, *78*, 192–201. https://doi.org/10.1205/026387600527220.

32. Sabiha, M.A.; Saidur, R.; Mekhilef, S.; Mahian, O. Progress and latest developments of evacuated tube solar collectors. *Renew. Sustain. Energy Rev.* **2015**, *51*, 1038–1054. https://doi.org/10.1016/j.rser.2015.07.016.
33. King Abdullah City for Atomic and Renewable Energy (K.A.CARE), Saudi Arabia. Renewable Resource Atlas. Available online: rratlas.energy.gov.sa (accessed on 20 April 2021)
34. Wyrwa, A.; Chen, Y.K. Techno-Economic Analysis of Adsorption-Based DH Driven Cooling System. *IOP Conf. Ser. Earth Environ. Sci.* **2019**, *214*, 012128. https://doi.org/10.1088/1755-1315/214/1/012128.
35. El-Shaarawi, M.A.; Al-Ugla, A.A. Unsteady analysis for solar-powered hybrid storage LiBr-water absorption air-conditioning. *Sol. Energy* **2017**, *144*, 556–568. https://doi.org/10.1016/j.solener.2016.12.054.
36. American Society for Heating, Refrigeration, and Air-Conditioning Engineers (ASHRAE). *Standard 62.1-2016 e Ventilation for Acceptable Indoor Air Quality*; Atlanta, GA, USA, 2016.
37. American Society of Heating, Refrigerating and Air-Conditioning Engineers (ASHRAE). International Weather for Energy Calculations (IWEC) V 2.0; Atlanta, GA, USA, 2012.
38. Asadi, J.; Amani, P.; Amani, M.; Kasaeian, A.; Bahiraei, M. Thermo-economic analysis and multi-objective optimization of absorption cooling system driven by various solar collectors. *Energy Convers. Manag.* **2018**, *173*, 715–727. https://doi.org/10.1016/j.enconman.2018.08.013.
39. Bry-Air. Dehumidification and environment control solutions. Available online: www.bryair.com (accessed on 9 February 2021).
40. Carrier - Saudi Arabia. Air conditioning, heating and refrigeration solutions. Available online: www.carrier.com/commercial/en/sa (accessed on 9 February 2021).